

# Novel calibrations of virial black hole mass estimators in active galaxies based on X–ray luminosity and optical/NIR emission lines

F. Ricci<sup>1</sup>, F. La Franca<sup>1</sup>, F. Onori<sup>2,3</sup>, and S. Bianchi<sup>1</sup>

<sup>1</sup> Dipartimento di Matematica e Fisica, Università Roma Tre, via della Vasca Navale 84, 00146 Roma, Italy  
e-mail: riccif@fis.uniroma3.it

<sup>2</sup> SRON, Netherlands Institute for Space Research, Sorbonnelaan 2, 3584 CA, Utrecht, the Netherlands

<sup>3</sup> Department of Astrophysics/IMAPP, Radboud University, P.O. Box9010, 6500 GL Nijmegen, the Netherlands

Received July 25, 2016; accepted October 4, 2016

## ABSTRACT

**Context.** Accurately weigh the masses of super massive black holes (BHs) in active galactic nuclei (AGN) is currently possible for only a small group of local and bright broad-line AGN through reverberation mapping (RM). Statistical demographic studies can be carried out considering the empirical scaling relation between the size of the broad line region (BLR) and the AGN optical continuum luminosity. However, there are still biases against low-luminosity or reddened AGN, in which the rest-frame optical radiation can be severely absorbed or diluted by the host galaxy and the BLR emission lines could be hard to detect.

**Aims.** Our purpose is to widen the applicability of virial-based single-epoch (SE) relations to reliably measure the BH masses also for low-luminosity or intermediate/type 2 AGN that are missed by current methodology. We achieve this goal by calibrating virial relations based on unbiased quantities: the hard X–ray luminosities, in the 2–10 keV and 14–195 keV bands, that are less sensitive to galaxy contamination, and the full-width at half-maximum (FWHM) of the most important rest-frame near-infrared (NIR) and optical BLR emission lines.

**Methods.** We built a sample of RM AGN having both X–ray luminosity and broad optical/NIR FWHM measurements available in order to calibrate new virial BH mass estimators.

**Results.** We found that the FWHM of the H $\alpha$ , H $\beta$  and NIR lines (i.e. Pa $\alpha$ , Pa $\beta$  and He I  $\lambda$ 10830) all correlate each other having negligible or small offsets. This result allowed us to derive virial BH mass estimators based on either the 2–10 keV or 14–195 keV luminosity. We took also into account the recent determination of the different virial coefficients  $f$  for pseudo and classical bulges. By splitting the sample according to the bulge type and adopting separate  $f$  factors (Ho & Kim 2014) we found that our virial relations predict BH masses of AGN hosted in pseudobulges  $\sim 0.5$  dex smaller than in classical bulges. Assuming the same average  $f$  factor for both population, a difference of  $\sim 0.2$  dex is still found.

**Key words.** Galaxies: active – Galaxies: nuclei – Galaxies: bulges – quasars: emission lines – quasars: supermassive black holes – X-rays: galaxies

## 1. Introduction

Supermassive black holes (SMBHs; having black hole masses  $M_{\text{BH}} = 10^5 - 10^9 M_{\odot}$ ) are observed to be common, hosted in the central spheroid in the majority of local galaxies. This discovery, combined with the observation of striking empirical relations between BH mass and host galaxy properties, opened in the last two decades an exciting era in extragalactic astronomy. In particular the realization that BH mass correlates strongly with the stellar luminosity, mass and velocity dispersion of the bulge (Dressler 1989; Kormendy & Richstone 1995; Magorrian et al. 1998; Ferrarese & Merritt 2000; Gebhardt et al. 2000; Marconi & Hunt 2003; Sani et al. 2011; Graham 2016, for a review) suggests that SMBHs may play a crucial role in regulating many aspects of galaxy formation and evolution (e.g. through AGN feedback, Silk & Rees 1998; Fabian 1999; Di Matteo et al. 2005; Croton et al. 2006; Sijacki et al. 2007; Ostriker et al. 2010; Fabian 2012; King 2014).

One of the most reliable and direct ways to measure the mass of a SMBH residing in the nucleus of an active galaxy (i.e. an active galactic nucleus, AGN) is reverberation mapping (RM,

Blandford & McKee 1982; Peterson 1993). The RM technique takes advantage of AGN flux variability to constrain black hole masses through time-resolved observations. With this method, the distance  $R = c\tau$  of the Broad Line Region (BLR) is estimated by measuring the time lag  $\tau$  of the response of a permitted broad emission line to variation of the photoionizing primary continuum emission. Under the hypothesis of a virialized BLR, whose dynamics are gravitationally dominated by the central SMBH,  $M_{\text{BH}}$  is simply related to the velocity of the emitting gas clouds,  $\Delta v$ , and to the size  $R$  of the BLR, i.e.  $M_{\text{BH}} = \Delta v^2 R G^{-1}$ , where  $G$  is the gravitational constant. Usually the width  $\Delta W$  of a doppler-broadened emission line (i.e. the full-width at half-maximum, FWHM, or the line dispersion,  $\sigma_{\text{line}}$ ) is used as a proxy of the real gas velocity  $\Delta v$ , after introducing a virial factor  $f$  which takes into account our ignorance on the structure, geometry and kinematics of the BLR (Ho 1999; Wandel et al. 1999; Kaspi et al. 2000)

$$M_{\text{BH}} = f \frac{\Delta W^2 R}{G}. \quad (1)$$

Operatively, the RM BH mass is equal to  $f \times M_{\text{vir}}$ , where the virial mass  $M_{\text{vir}}$  is  $\Delta W^2 R G^{-1}$ . In the last decade, the  $f$  factor has been studied by several authors, finding values in the range 2.8 – 5.5 (if the line dispersion  $\sigma_{\text{line}}$  is used, see e.g. Onken et al. 2004; Woo et al. 2010; Graham et al. 2011; Park et al. 2012; Grier et al. 2013). This quantity is statistically determined by normalizing the RM AGN to the relation between BH mass and bulge stellar velocity dispersion ( $M_{\text{BH}} - \sigma_{\star}$  relation; see Ferrarese 2002; Tremaine et al. 2002; Hu 2008; Gültekin et al. 2009; Graham & Scott 2013; McConnell & Ma 2013; Kormendy & Ho 2013; Savorgnan & Graham 2015; Sabra et al. 2015) observed in local inactive galaxies with direct BH mass measurements. However, recently Shankar et al. (2016) claimed that the previously computed  $f$  factors could have been artificially increased by a factor of at least  $\sim 3$  because of a presence of a selection bias in the calibrating samples, in favour of the more massive BHs. Kormendy & Ho (2013) significantly updated the  $M_{\text{BH}} - \sigma_{\star}$  relation for inactive galaxies, highlighting a large and systematic difference between the relations for pseudo and classical bulges/ellipticals. It should be noted that the classification of galaxies into classical and pseudo bulges is a difficult task<sup>1</sup>, which depends on a number of selection criteria, which should not be used individually (e.g. not only the Sersic index (Sersic 1968)  $n < 2$  condition to classify a source as a pseudo bulge; see Kormendy & Ho 2013; Kormendy 2016).

The results on the  $M_{\text{BH}} - \sigma_{\star}$  found by Kormendy & Ho (2013) prompted Ho & Kim (2014) to calibrate the  $f$  factor separately for the two bulge populations (for a similar approach see also Graham et al. 2011, that derived different  $M_{\text{BH}} - \sigma_{\star}$  relations and  $f$  factors for barred and non-barred galaxies), getting  $f_{\text{CB}} = 6.3 \pm 1.5$  for elliptical/classical and  $f_{\text{PB}} = 3.2 \pm 0.7$  for pseudo bulges when the  $\text{H}\beta$   $\sigma_{\text{line}}$  (not the FWHM)<sup>2</sup> is used to compute the virial mass.

However, RM campaigns are time-consuming and are accessible only for a handful of nearby (i.e.  $z \lesssim 0.1$ ) AGN. The finding of a tight relation between the distance of the BLR clouds  $R$  and the AGN continuum luminosity  $L$  ( $R \propto L^{0.5}$ , Bentz et al. 2006, 2013), has allowed to calibrate new single-epoch (SE) relations that can be used on larger samples of AGN, such as

$$\log\left(\frac{M_{\text{BH}}}{M_{\odot}}\right) = a + b \log\left[\left(\frac{L}{10^{42} \text{ erg s}^{-1}}\right)^{0.5} \left(\frac{\text{FWHM}}{10^4 \text{ km s}^{-1}}\right)^2\right]; \quad (2)$$

where the term  $\log(L^{0.5} \times \text{FWHM}^2)$  is generally known as virial product (VP). These SE relations have a typical spread of  $\sim 0.5$  dex (e.g. McLure & Jarvis 2002; Vestergaard & Peterson 2006) and are calibrated using either the broad emission line or the continuum luminosity (e.g. in the ultraviolet and optical, mostly at 5100 Å,  $L_{5100}$ ; see the review by Shen 2013, and references therein) and the FWHM (or the  $\sigma_{\text{line}}$ ) of optical emission lines<sup>3</sup>,

<sup>1</sup> Some authors have also discussed how could be neither appropriate nor possible to reliably separate bulges into one class or another (Graham 2014), and that in some galaxies there is evidence of coexistence of classical bulges and pseudobulges (Erwin et al. 2015; Dullo et al. 2016).

<sup>2</sup> Note that if the FWHM instead of the  $\sigma_{\text{line}}$  is used, the virial coefficient  $f$  has to be properly scaled depending on the FWHM/ $\sigma_{\text{line}}$  ratio (see e.g. Onken et al. 2004; Collin et al. 2006, for details).

<sup>3</sup> As the calibrating RM masses are computed by measuring the BLR line width and its average distance  $R = c\tau$ , the fit of Equation 2 corresponds, strictly speaking, to the fit of the  $\tau$  versus  $L$  relation (e.g. Bentz et al. 2006).

such as  $\text{H}\beta$ ,  $\text{Mg II } \lambda 2798$ ,  $\text{C IV } \lambda 1549$  (even though the latter is still debated; e.g. Baskin & Laor 2005; Shen & Liu 2012; Denney 2012; Runnoe et al. 2013).

These empirical scaling relations have some problems though:

- Broad Fe II emission in type 1 AGN (AGN1) can add ambiguity in the determination of the optical continuum luminosity at 5100 Å.
- In low-luminosity AGN, host galaxy starlight dilution can severely affect the AGN ultraviolet and optical continuum emission. Therefore in such sources it becomes very challenging, if not impossible at all, to isolate the AGN contribution unambiguously.
- The  $\text{H}\beta$  transition is at least a factor of three weaker than  $\text{H}\alpha$  and so from considerations of signal-to-noise ratio (S/N) alone,  $\text{H}\alpha$ , if available, is superior to  $\text{H}\beta$ . In practice, in some cases  $\text{H}\alpha$  may be the only line with a detectable broad component in the optical (such objects are known as Seyfert 1.9 galaxies; Osterbrock 1981).
- The optical SE scaling relations are completely biased against type 2 AGN (AGN2) which lack broad emission lines in the rest-frame optical spectra. However, several studies have shown that most AGN2 exhibit faint components of broad lines if observed with high ( $\gtrsim 20$ ) S/N in the rest-frame near-infrared (NIR), where the dust absorption is less severe than in the optical (Veilleux et al. 1997; Riffel et al. 2006; Cai et al. 2010; Onori et al. 2016). Moreover, some studies have shown that NIR lines (i.e.  $\text{Pa}\alpha$  and  $\text{Pa}\beta$ ) can be reliably used to estimate the BH masses in AGN1 (Kim et al. 2010, 2015; Landt et al. 2013) and also for intermediate/type 2 AGN (La Franca et al. 2015, 2016).

In an effort to widen the applicability of this kind of relations to classes of AGN that would otherwise be inaccessible using the conventional methodology (e.g. galaxy-dominated low-luminosity sources, type 1.9 Seyfert and type 2 AGN), La Franca et al. (2015) fitted new virial BH mass estimators based on intrinsic (i.e. absorption corrected) hard, 14–195 keV, X–ray luminosity, which is thought to be produced by the hot corona via Compton scattering of the ultraviolet and optical photons coming from the accretion disk (Haardt & Maraschi 1991; Haardt et al. 1994, 1997). Actually the X–ray luminosity  $L_X$  is known to be empirically related to the dimension of the BLR, as it is observed for the optical continuum luminosity of the AGN accretion disk (e.g. Maiolino et al. 2007; Greene et al. 2010). Thanks to these  $R - L_X$  empirical scaling relations, also Bongiorno et al. (2014) have derived virial relations based on the  $\text{H}\alpha$  width and on the hard, 2–10 keV, X–ray luminosity, that is less affected by galaxy obscuration (excluding severely absorbed, Compton Thick, AGN:  $N_{\text{H}} > 10^{24} \text{ cm}^{-2}$ ). Indeed in the 14–195 keV band up to  $N_{\text{H}} < 10^{24} \text{ cm}^{-2}$  the absorption is negligible while in the 2–10 keV band the intrinsic X–ray luminosity can be recovered after measuring the  $N_{\text{H}}$  column density via X–ray spectral fitting.

Recently Ho & Kim (2015) showed that the BH masses of RM AGN correlates tightly and linearly with the optical VP (i.e.  $\text{FWHM}(\text{H}\beta)^2 \times L_{5100}^{0.5}$ ) with different logarithmic zero points for elliptical/classical and pseudo bulges. They used the updated database of RM AGN with bulge classification from Ho & Kim (2014) and adopted the virial factors separately for classical ( $f_{\text{CB}} = 6.3$ ) and pseudobulges ( $f_{\text{PB}} = 3.2$ ).

Prompted by these results, in this paper we present an update of the calibrations of the virial relations based on the hard 14–195 keV X–ray luminosity published in La Franca et al. (2015).

We extend these calibrations to the 2-10 keV X-ray luminosity and to the most intense optical and NIR emission lines, i.e.  $H\beta$   $\lambda 4862.7$  Å,  $H\alpha$   $\lambda 6564.6$  Å,  $He I$   $\lambda 10830.0$  Å,  $Pa\beta$   $\lambda 12821.6$  Å and  $Pa\alpha$   $\lambda 18756.1$  Å. In order to minimize the statistical uncertainties in the estimate of the parameters  $a$  and  $b$  of the virial relation (Equation 2), we have verified that reliable statistical correlations do exist among the hard X-ray luminosities,  $L_{2-10\text{keV}}$  and  $L_{14-195\text{keV}}$ , and among the optical and NIR emission lines (as already found by other studies: Greene & Ho 2005; Landt et al. 2008; Mejía-Restrepo et al. 2016). These correlations allowed us 1) to compute, using the total dataset, average FWHM and  $L_X$  for each object and then derive more statistically robust virial relations and 2) to compute our BH mass estimator using any combination of  $L_X$  and optical or NIR emission line width.

We will proceed as follows: Sect. 2 presents the RM AGN dataset; in Sect. 3 we will test whether the optical (i.e.  $H\alpha$  and  $H\beta$ ) and NIR (i.e.  $Pa\alpha$ ,  $Pa\beta$  and  $He I$   $\lambda 10830$  Å, hereafter  $He I$ ) emission lines probe similar region in the BLR; in Sect. 4 new calibrations of the virial relations based on the average hard X-ray luminosity and the average optical/NIR emission lines width, taking (or not) into account the bulge classification, are presented; finally Sect. 5 addresses the discussion of our findings and the conclusions. Throughout the paper we assume a flat  $\Lambda$ CDM cosmology with cosmological parameters:  $\Omega_\Lambda = 0.7$ ,  $\Omega_M = 0.3$  and  $H_0 = 70$  km s<sup>-1</sup> Mpc<sup>-1</sup>. Unless otherwise stated, all the quoted uncertainties are at 68% ( $1\sigma$ ) confidence level.

## 2. Data

As we are interested in expanding the applicability of SE relations, we decided to use emission lines that can be more easily measured also in low-luminosity or obscured sources, such as the  $H\alpha$  or the  $Pa\alpha$ ,  $Pa\beta$  and  $He I$ . Moreover, we want also to demonstrate that such lines can give reliable estimates as the  $H\beta$  (see e.g. Greene & Ho 2005; Landt et al. 2008; Kim et al. 2010; Mejía-Restrepo et al. 2016). For this reason, we built our sample starting from the database of Ho & Kim (2014) that lists 43 RM AGN (i.e. ~90% of all the RM black hole masses available in the literature), all having bulge type classifications based on the criteria of Kormendy & Ho (2013, Supplemental Material). In particular, Ho & Kim (2014) used the most common condition to classify as classical bulges those galaxies having Sersic index (Sersic 1968)  $n < 2$ . However when the nucleus is too bright this condition is not totally reliable due to the difficulty of carefully measure the bulge properties. In this case Ho & Kim (2014) adopted the condition that the bulge-to-total light fraction should be  $\leq 0.2$  (e.g. Fisher & Drory 2008; Gadotti 2009, but see Graham & Worley 2008 for a discussion on the uncertainties of this selection criterion). In some cases, additional clues came from the detection of circumnuclear rings and other signatures of ongoing central star formation.

It should be noted that an offset ( $\sim 0.3$  dex) is observed in the  $M_{BH} - \sigma_*$  diagram both when the galaxies are divided into barred and unbarred (e.g. Graham 2008; Graham et al. 2011; Graham & Scott 2013) and into classical and pseudobulges (Hu 2008). However, the issue on the bulge type classification and on which host properties better discriminate the  $M_{BH} - \sigma_*$  relation is beyond the scope of this work, and in the following we will adopt the bulge type classification as described in Ho & Kim (2014).

Among this sample, we selected those AGN having hard X-ray luminosity and at least one emission line width available among  $H\beta$ ,  $H\alpha$ ,  $Pa\alpha$ ,  $Pa\beta$  and  $He I$ . The data of 3C 390.3

were excluded since it clearly shows a double-peaked  $H\alpha$  profile (Burbidge & Burbidge 1971; Dietrich et al. 2012), a feature that could be a sign of non-virial motions (in particular of accretion disk emission, e.g. Eracleous & Halpern 1994, 2003; Gezari et al. 2007). Therefore our dataset is composed as follows:

1.  $H\beta$  sample. The largest sample considered in this work includes 39 RM AGN with  $H\beta$  FWHM coming either from a mean or a single spectrum. By requiring that these AGN have an X-ray luminosity measured either in the 2-10 keV or 14-195 keV band reduces the sample to 35 objects.
2.  $H\alpha$  sample. Thirty-two<sup>4</sup> AGN have  $H\alpha$  FWHM. Among this sample, Mrk 877 and SBS 1116+583A do not have an  $L_X$  measurement available. Thus the final sample having both  $H\alpha$  FWHM and X-ray luminosity includes 30 galaxies.
3. NIR sample. The FWHM of the NIR emission lines were taken from Landt et al. (2008, 2013, i.e. 19  $Pa\alpha$ , 20  $Pa\beta$  and 16  $He I$ ). We added the measurements of NGC 3783 that we observed simultaneously in the ultraviolet, optical and NIR with Xshooter (Onori et al. 2016). Therefore the total NIR sample, with available X-ray luminosity, counts: 19  $Pa\alpha$ , 21  $Pa\beta$  and 17  $He I$ .

The details of each RM AGN are reported in Table 1. The intrinsic hard X-ray luminosities have been taken either from the SWIFT/BAT 70 month catalogue (14-195 keV,  $L_{14-195\text{keV}}$ ; Baumgartner et al. 2013), or from the CAIXA catalogue (2-10 keV,  $L_{2-10\text{keV}}$ ; Bianchi et al. 2009). PG 1411+442 has public 2-10 keV luminosity from Piconcelli et al. (2005), while Mrk 1310 and NGC 4748 have public XMM observations, therefore we derived their 2-10 keV luminosity via X-ray spectral fitting. Both X-ray catalogues list the 90% confidence level uncertainties on the  $L_X$  and/or on the hard X-ray fluxes, which were converted into the  $1\sigma$  confidence level. For PG 1411+442, as the uncertainty on the  $L_{2-10\text{keV}}$  has not been published (Piconcelli et al. 2005), a 6% error (equivalent to 10% at the 90% confidence level) has been assumed. All the FWHMs listed in Table 1 have been corrected for the instrumental resolution broadening. When possible, we always preferred to use coeval (i.e. within few months) FWHM measurements of the NIR and optical lines. This choice is dictated by the aim of verifying whether the optical and NIR emission lines are originated at similar distance in the BLR. The virial masses have been taken mainly from the compilations of Grier et al. (2013) and Ho & Kim (2014), and were computed from the  $\sigma_{\text{line}}(H\beta)$ , measured from the root-mean-square (rms) spectra taken during RM campaigns, and the updated  $H\beta$  time lags (see Zu et al. 2011; Grier et al. 2013). For 3C 273 and Mrk 335 the logarithmic mean of the measurements available (Ho & Kim 2014) were used.

To the data presented in Table 1, we also added six AGN1 from Landt et al. (2008, 2013) (see Table 2) without neither RM  $M_{BH}$  nor bulge classification, that however have simultaneous measurements of optical and/or NIR lines. They are, namely: H 1821+643, H 1934-063, H 2106-099, HE 1228+013, IRAS 1750+508, PDS 456. Table 2 also lists the optical data of Mrk 877 and SBS 1116+583A. These additional eight sources that do not appear in Table 1 are used only in the next Section in which emission line relations are investigated.

<sup>4</sup> The AGN having  $H\alpha$  FWHM are 33, but we excluded the source Mrk 202 as the  $H\alpha$  FWHM is deemed to be unreliable (Bentz et al. 2010).

**Table 1.** Properties of the RM AGN with both bulge classification and hard X-ray luminosity.

Galaxy	$\log L_{2-10\text{keV}}$ [erg s <sup>-1</sup> ]	$\log L_{14-195\text{keV}}$ [erg s <sup>-1</sup> ]	FWHM H $\beta$ [km s <sup>-1</sup> ]	FWHM H $\alpha$ [km s <sup>-1</sup> ]	FWHM Pa $\alpha$ [km s <sup>-1</sup> ]	FWHM Pa $\beta$ [km s <sup>-1</sup> ]	FWHM He I [km s <sup>-1</sup> ]	ref OPT/NIR	$M_{\text{vir}}$ [10 <sup>6</sup> M <sub>⊙</sub> ]	ref $M_{\text{vir}}$	Bulge type
(1)	(2)	(3)	(4)	(5)	(6)	(7)	(8)	(9)	(10)	(11)	(12)
3C 120	44.06	44.38	1430	2168	...	2727	...	G12,K14/L13	12.2 <sup>+0.9</sup> <sub>-0.9</sub>	G13	CB
3C 273	45.80	46.48	3943	2773	2946	2895	3175	L08,K00/L08	161 <sup>+34</sup> <sub>-34</sub>	P04	CB
Ark 120	43.96	44.23	5927	4801	5085	5102	4488	L08	23.4 <sup>+4.0</sup> <sub>-5.7</sub>	G13	CB
Arp 151	...	43.30	3098	1852	...	...	...	B09,B10	1.1 <sup>+0.2</sup> <sub>-0.1</sub>	G13	CB
Fairall 9	43.78	44.41	6000	...	...	...	...	P04	54.3 <sup>+11.8</sup> <sub>-11.6</sub>	HK14	CB
Mrk 79	43.11	43.72	3679	3921	3401	3506	2480 <sup>†</sup>	L08	19.2 <sup>+4.5</sup> <sub>-7.4</sub>	G13	CB
Mrk 110	43.91	44.22	2282	1954	1827	1886	1961	L08	5.2 <sup>+1.3</sup> <sub>-2.1</sub>	G13	CB
Mrk 279	...	43.92	5354	...	...	3546	...	P04/L13	7.2 <sup>+1.1</sup> <sub>-1.1</sub>	G13	PB
Mrk 290	43.08	43.67	5066	4261	3542	4228	3081	L08	3.9 <sup>+0.4</sup> <sub>-0.3</sub>	HK14	CB
Mrk 335	43.44	43.45	2424	1818	1642	1825	1986	L08	2.98 <sup>+0.63</sup> <sub>-0.68</sub>	HK14	CB
Mrk 509	44.02	44.42	3947	3242	3068	3057	2959	L08	22.2 <sup>+1.0</sup> <sub>-1.0</sub>	G13	CB
Mrk 590	43.04	43.42	9874 <sup>†</sup>	4397	4727	3949	3369	L08	7.3 <sup>+1.2</sup> <sub>-1.6</sub>	G13	PB
Mrk 771	43.47	44.11	3828	2924	...	...	...	P04,K00	16.0 <sup>+2.7</sup> <sub>-2.6</sub>	G13	PB
Mrk 817	43.46	43.77	6732	5002	4665	5519	4255	L08	14.6 <sup>+2.2</sup> <sub>-2.5</sub>	G13	PB
Mrk 876	44.23	44.73	8361	...	5505	6010	5629	L08	50.8 <sup>+21.3</sup> <sub>-21.5</sub>	P04	CB
Mrk 1310	41.34	42.98	2409	561 <sup>†</sup>	...	...	...	B09,B10	0.47 <sup>+0.20</sup> <sub>-0.17</sub>	G13	CB
Mrk 1383	44.18	44.52	7113	5430	...	...	...	P04,K00	373.3 <sup>+68.7</sup> <sub>-71.3</sub>	G13	CB
Mrk 1513	43.56	...	1781	...	1862	...	...	G12/L13	22.7 <sup>+3.4</sup> <sub>-3.4</sub>	HK14	PB
NGC 3227	41.57	42.56	3939	3414	...	2934	3007	L08	5.2 <sup>+2.0</sup> <sub>-2.1</sub>	G13	PB
NGC 3516	42.46	43.31	...	...	...	4451	...	L13	7.2 <sup>+0.7</sup> <sub>-0.6</sub>	G13	PB
NGC 3783	43.08	43.58	5549	5290	...	3500	5098	On+	4.4 <sup>+0.7</sup> <sub>-0.8</sub>	G13	PB
NGC 4051	41.44	41.67	...	...	...	1633	...	L13	0.5 <sup>+0.1</sup> <sub>-0.1</sub>	G13	PB
NGC 4151	42.53	43.12	4859	5248	...	4654	2945 <sup>†</sup>	L08	8.4 <sup>+0.9</sup> <sub>-0.5</sub>	G13	CB
NGC 4253	42.93	42.91	1609	1013	...	...	...	B09,B10	0.3 <sup>+0.2</sup> <sub>-0.2</sub>	G13	PB
NGC 4593	42.87	43.20	4341	3723	...	3775	3232	L08	2.1 <sup>+0.4</sup> <sub>-0.3</sub>	G13	PB
NGC 4748	42.63	42.82	1947	1967	...	...	...	B09,B10	0.7 <sup>+0.2</sup> <sub>-0.2</sub>	G13	PB
NGC 5548	43.42	43.72	10000 <sup>†</sup>	5841	4555	6516	6074	L08	13.8 <sup>+1.7</sup> <sub>-2.0</sub>	G13	CB
NGC 6814	42.14	42.67	3323	2909	...	...	...	B09,B10	3.7 <sup>+0.5</sup> <sub>-0.5</sub>	G13	PB
NGC 7469	43.23	43.60	1952	2436	450 <sup>†</sup>	1758	1972	L08	4.8 <sup>+1.4</sup> <sub>-1.4</sub>	G13	PB
PG 0026+129	...	44.83	2544	1457	1748	...	...	P04,K00/L13	56.8 <sup>+13.6</sup> <sub>-12.9</sub>	HK14	CB
PG 0052+251	44.64	44.95	5008	2651	4114	...	...	P04,K00/L13	92.6 <sup>+6.8</sup> <sub>-6.4</sub>	HK14	CB
PG 0804+761	44.44	44.57	3053	2719	2269	...	...	P04,K00/L13	88.5 <sup>+6.9</sup> <sub>-8.7</sub>	HK14	CB
PG 0844+349	43.70	...	2288	1991	2183	2377	2101	L08	5.0 <sup>+2.2</sup> <sub>-0.7</sub>	HK14	CB
PG 0953+414	44.69	...	3071	...	...	...	...	P04	54.0 <sup>+8.5</sup> <sub>-8.5</sub>	HK14	CB
PG 1211+143	43.73	...	2012	1407	1550	...	...	P04,K00/L13	16.7 <sup>+2.2</sup> <sub>-6.2</sub>	HK14	CB
PG 1307+085	44.08	...	5059	3662	2955	...	...	P04,K00/L13	122 <sup>+12.1</sup> <sub>-11.8</sub>	HK14	CB
PG 1411+442	43.40	...	2801	2123	...	...	...	P04,K00	26.9 <sup>+7.7</sup> <sub>-4.8</sub>	HK14	CB

**Notes.** Columns are: (1) galaxy name; (2) and (3) logarithm of the 2-10 keV and 14-195 keV band luminosities; (4) to (8) are the FWHMs of H $\beta$ , H $\alpha$ , Pa $\alpha$ , Pa $\beta$  and He I; (9) references for the optical and NIR emission lines, where: G12 is Grier et al. (2012), K14 is Kollatschny et al. (2014), L13 is Landt et al. (2013), L08 is Landt et al. (2008), K00 is Kaspi et al. (2000), B09 is Bentz et al. (2009), B10 is Bentz et al. (2010), P04 is Peterson et al. (2004), On+ is Onori et al. (2016); (10) virial BH masses (to be multiplied for the virial  $f$  factor in order to obtain the black hole mass  $M_{\text{BH}}$ ); (11) references for the virial masses, where: G13 is Grier et al. (2013), HK14 is Ho & Kim (2014) and the other labels are the same used in the references of column (9); (12) bulge classification of each galaxy, CB = classical bulge or elliptical; PB = pseudobulge. From compilation of Ho & Kim (2014), which also contains references to original data sources.

(<sup>†</sup>) Measurements considered outliers, see Sect. 3 for more details.

**Table 2.** Properties of the additional AGN1 database used in the emission line relation analysis.

Galaxy	FWHM H $\beta$ [km s $^{-1}$ ]	FWHM H $\alpha$ [km s $^{-1}$ ]	FWHM Pa $\alpha$ [km s $^{-1}$ ]	FWHM Pa $\beta$ [km s $^{-1}$ ]	FWHM He I [km s $^{-1}$ ]	ref OPT/NIR
(1)	(2)	(3)	(4)	(5)	(6)	(7)
H 1821+643	6615	5051	...	5216	4844	L08
H 1934-063	1683	1482	1354	1384	1473	L08
H 2106-099	2890	2368	1723	2389	2553	L08
HE 1228+013	2152	1857	1916	1923	1770	L08
IRAS 1750+508	2551	2323	...	1952	1709	L08
Mrk 877	6641	4245	...	...	...	K00,P04
PDS 456	3159	...	2022	2068	...	L08
SBS 1116+583A	3668	2059	...	...	...	B09,B10

**Notes.** Columns are: (1) galaxy name; (2) to (6) are the FWHMs of H $\beta$ , H $\alpha$ , Pa $\alpha$ , Pa $\beta$  and He I; (7) references for the optical and NIR emission lines, where: L08 is Landt et al. (2008), K00 is Kaspi et al. (2000), P04 is Peterson et al. (2004), B09 is Bentz et al. (2009) and B10 is Bentz et al. (2010).

### 3. Emission line relations

As suggested by several works (e.g. Greene & Ho 2005; Shen & Liu 2012; Mejía-Restrepo et al. 2016), the strongest Balmer lines, H $\alpha$  and H $\beta$ , seem to come from the same area of the BLR. If we confirm that a linear correlation between H I and He I optical and NIR lines (i.e. Pa $\alpha$ , Pa $\beta$  and He I) does exist, this has two consequences: it will indicate i) that these lines come from the same region of the BLR, and ii) that the widely assumed virialization of H $\beta$  also implies the virialization of H $\alpha$  and of the NIR lines.

Figure 1 shows the results of our analysis, by comparing the FWHM of H $\alpha$  with the FWHMs of the H $\beta$ , Pa $\alpha$ , Pa $\beta$  and He I lines. In all panels the coeval FWHMs are shown by red filled circles while those not coeval by black filled circles. Although in some cases the uncertainties are reported in the literature, following the studies of Grupe et al. (2004), Vestergaard & Peterson (2006), Landt et al. (2008), Denney et al. (2009), we assumed a common uncertainty of 10% on the FWHM measurements.

The top left panel of Fig. 1 shows the relation between the two Balmer emission lines. We find a good agreement between the FWHMs of H $\alpha$  and H $\beta$ . Using the sub-sample of 23 sources with simultaneous measurements, the Pearson correlation coefficient results to be  $r \simeq 0.92$ , with a probability of being drawn from an uncorrelated parent population as low as  $\sim 6 \times 10^{-10}$ . The least-squares problem was solved using the symmetrical regression routine FITEXY (Press et al. 2007) that can incorporate errors on both variables and allows us to account for intrinsic scatter. We fitted a log-linear relation to the simultaneous sample and found

$$\log FWHM(H\alpha) = \log FWHM(H\beta) - (0.075 \pm 0.013). \quad (3)$$

The above relation means that H $\beta$  is on average 0.075 dex broader than H $\alpha$ , with a scatter of  $\sim 0.08$  dex. This relation has a reduced  $\chi^2_v \simeq 1.68$ . We performed the F-test to verify the significance of this non-zero offset with respect to a 1:1 relation, getting a probability value of  $\sim 2e-4$  that the improvement of the fit was obtained by chance<sup>5</sup>. Therefore in this case the relation with a non-zero offset resulted to be highly significant. We also tested whether this offset changes according to the bulge classification, when available. No significant difference was found, as

<sup>5</sup> Throughout this work in the F-test we use a threshold of 0.012, corresponding to a  $2.5\sigma$  Gaussian deviation, in order to rule out the introduction of an additional fitting parameter.

the offset of the pseudo bulges resulted to be  $0.076 \pm 0.020$  and for the classical/elliptical  $0.074 \pm 0.020$ .

Equation 3 is shown as a red solid line in the top left panel of Fig. 1. Our result is in fair agreement (i.e. within  $2\sigma$ ) with other independent estimates, that are shown as cyan (Greene & Ho 2005) and blue (Mejía-Restrepo et al. 2016) dashed lines. If instead we consider the total sample of 34 AGN having both H $\alpha$  and H $\beta$  measured (i.e. including also non-coeval FWHMs), we get an average offset of  $0.091 \pm 0.010$  with a larger scatter ( $\sim 0.1$  dex). Also in this case, the offset does not show a statistically significant dependence on the bulge classification, as the offset of elliptical/classical bulges resulted to be  $0.102 \pm 0.014$  and for pseudo bulges it resulted to be  $0.080 \pm 0.019$ . In all the aforementioned fits, three outliers<sup>6</sup> have been excluded even though the FWHMs were measured simultaneously. The excluded galaxies namely are Mrk 1310, Mrk 590 and NGC 5548. The first one has been excluded because the H $\alpha$  measurement is highly uncertain ( $561^{+960}_{-136}$  km s $^{-1}$ , Bentz et al. 2010), the latter two have extremely broader H $\beta$  than either H $\alpha$ , Pa $\alpha$ , Pa $\beta$  and He I. This fact is due to the presence of a prominent “red shelf” in the H $\beta$  of these two sources (Landt et al. 2008). This red shelf is also most likely responsible for the average trend observed between H $\beta$  and H $\alpha$ , i.e. of H $\beta$  being on average broader than H $\alpha$  (Equation 3). Indeed it is well known (e.g. De Robertis 1985; Marziani et al. 1996, 2013) that the H $\beta$  broad component is in part blended with weak Fe II multiplets, He II  $\lambda 4686$  and He I  $\lambda 4922$ , 5016 (Véron et al. 2002; Kollatschny et al. 2001). The simultaneous sample gives a relation with lower scatter than the total sample. Indeed, the non-simultaneous measurements introduce additional noise due to the well-known AGN variability phenomenon. Therefore in the following Sections we will use the average offset between the FWHM of H $\alpha$  and H $\beta$  computed using the coeval sample (i.e. Equation 3), which also better agrees with the relations already published by Greene & Ho (2005) and Mejía-Restrepo et al. (2016).

The other three panels of Fig. 1 show the relations between the H $\alpha$  and the NIR emission lines Pa $\alpha$  (19 objects), Pa $\beta$  (22) and He I (19). When compared to H $\alpha$ , the samples have Pearson correlation coefficient  $r$  of 0.92, 0.94 and 0.95, with probabilities of being drawn from an uncorrelated parent population as low as  $\sim 2 \times 10^{-8}$ ,  $9 \times 10^{-11}$  and  $5 \times 10^{-10}$  for the Pa $\alpha$ , Pa $\beta$  and He I, respectively. No significant difference is seen between the emission line widths of H $\alpha$  and the NIR lines. This is not sur-

<sup>6</sup> The outlier values are marked with a dag in Table 1.

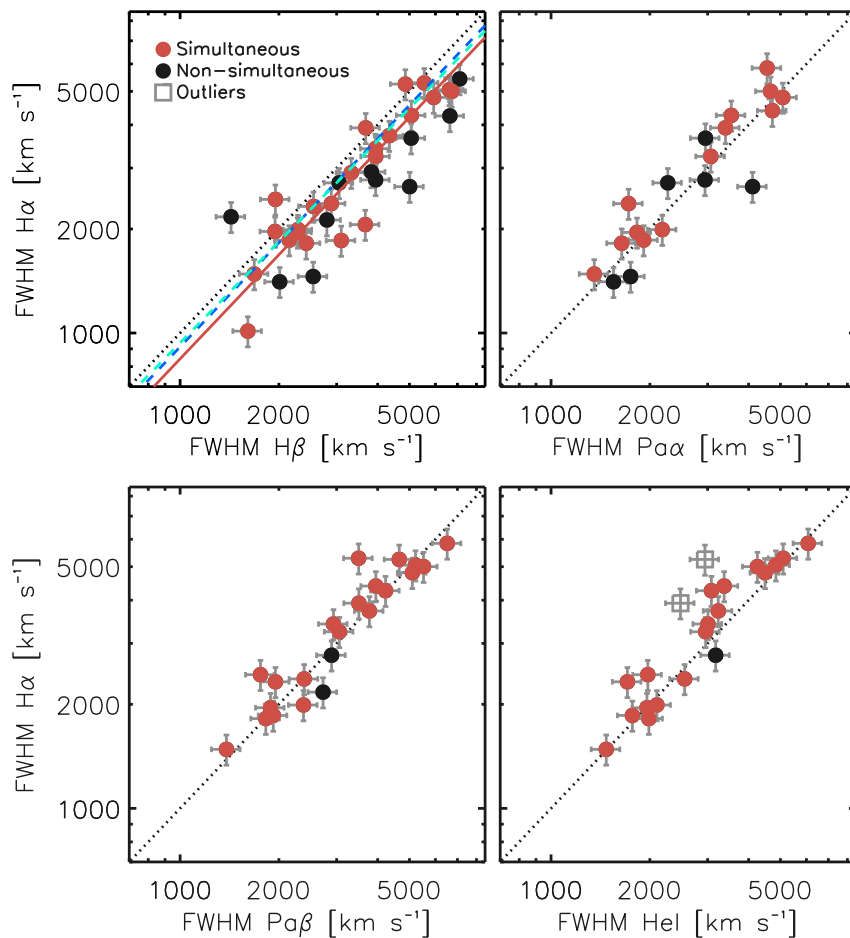


**Fig. 1.** Linear relations between the FWHM of  $H\alpha$  and the FWHM either of  $H\beta$ ,  $Pa\alpha$ ,  $Pa\beta$  or  $He\text{ I}$ , from left to right and top to bottom. Red filled circles denote simultaneous observations of the two lines, while black filled circles describe non-simultaneous line measurements. Grey open squares indicate the measurements that are classified as outliers (see text for more details) and are not considered in the fits. The black dotted line shows the 1:1 relation in all panels. In the top left panel, the best-fit relation computed on the coeval sample is shown as a red solid line. The relations from Greene & Ho (2005, dashed cyan) and Mejía-Restrepo et al. (2016, dashed blue) are also reported.

prising as already Landt et al. (2008) noted that there was a good agreement between the FWHM of the  $Pa\beta$  and the two strongest Balmer lines, though an average trend of  $H\beta$  being larger than  $Pa\beta$  was suggested (a quantitative analysis was not carried out). We fitted log-linear relations to the data and always found that the 1:1 relation is the best representation of the sample. We found a reduced  $\chi^2_\nu$  of 1.54, 1.12 and 1.14 for  $Pa\alpha$ ,  $Pa\beta$  and  $He\text{ I}$ , respectively. The F-test was carried out in order to quantitatively verify whether the equality relation is preferred with respect to relations either with a non-zero offset or also including a free slope. The improvements with a relation having free slope resulted not to be highly significant, and therefore the more physically motivated 1:1 relation was preferred. These best-fitting relations are shown as black dotted lines in the remaining three panels of Figure 1. The relation between  $H\alpha$  and the  $Pa\beta$  emission line has been fitted using the whole sample, while for the  $Pa\alpha$  and  $He\text{ I}$  correlations we excluded the sources: NGC 7469 (for the  $Pa\alpha$ ), Mrk 79 and NGC 4151 (for the  $He\text{ I}$ ; shown as grey open squares in the bottom right panel of Fig. 1). Although these three sources have simultaneous optical and NIR observations (Landt et al. 2008), all show significantly narrower width of the  $Pa\alpha$  or  $He\text{ I}$  than all the other available optical and NIR emission lines.

#### 4. Virial mass calibrations

In the previous Section we showed that the  $H\alpha$  FWHM is equivalent to the widths of the NIR emission lines,  $Pa\alpha$ ,  $Pa\beta$  and  $He\text{ I}$ , while it is on average 0.075 dex narrower than  $H\beta$ . In order to minimize the uncertainties on the estimate of the zero point and slope that appear in Equation 2 we used the whole dataset listed in Table 1. This is possible because, besides the linear correlations between the optical and NIR FWHMs, also the intrinsic hard X-ray luminosities  $L_{2-10\text{ keV}}$  and  $L_{14-195\text{ keV}}$  are correlated. Indeed, as expected in AGN, we found in our sample a relation between the two hard X-ray luminosities,

$$\log L_{2-10\text{ keV}} = \log L_{14-195\text{ keV}} - (0.567 \pm 0.004), \quad (4)$$

which corresponds to an average X-ray photon index  $\langle\Gamma\rangle \simeq 1.67$  ( $f_\nu \propto \nu^{-(\Gamma-1)}$ ). We can therefore calculate, for each object of our sample, a sort of average VP, which has been computed by using the average FWHM of the emission lines (the  $H\beta$  has been converted into  $H\alpha$  by using Equation 3) and the average X-ray luminosity (converted into 2-10 keV band using Equation 4). When computing the average FWHM, the values that in the previous Section were considered outliers were again excluded. However we note that each RM AGN has at least one valid FWHM measurement, therefore none of the AGN has been excluded. This

**Table 3.** Results of the fits of the virial relations.

$M_{\text{BH}}$ vs $VP(\langle FWHM(H\alpha) \rangle, \langle L_{2-10\text{keV}} \rangle)$							
sample	$a$	$b$	N	r	Prob(r)	$\epsilon_{\text{obs}}$	$\epsilon_{\text{intr}}$
(1)	(2)	(3)	(4)	(5)	(6)	(7)	(8)
All	$8.032 \pm 0.014$	$1^{(a)}$	37	0.838	$9 \times 10^{-11}$	0.40	0.38
Clas	$8.083 \pm 0.016$	$1^{(a)}$	23	0.837	$7 \times 10^{-7}$	0.38	0.37
Pseudo	$7.911 \pm 0.026$	$1^{(a)}$	14	0.731	$3 \times 10^{-3}$	0.40	0.38
All <sup>(b)</sup>	$8.187 \pm 0.021$	$1.376 \pm 0.033$	37	0.831	$2 \times 10^{-10}$	0.49	0.48

**Notes.** Best fitting parameters of the virial relations (see Equation 2) between the  $M_{\text{BH}} = f \times M_{\text{vir}}$ , with  $\langle f \rangle = 4.31$  (Grier et al. 2013), and the average VP given by the mean FWHM (once the  $H\beta$  has been converted into  $H\alpha$ ) and the mean  $L_{2-10\text{keV}}$  (using Equation 4 to convert  $L_{14-195\text{keV}}$ ). Columns are: (1) sample bulge type, (2) and (3) zero point and slope of the virial relation, (4) number of objects of each sample, (5) and (6) Pearson correlation coefficient with its t-student probability, (7) logarithmic spread of the data on the  $M_{\text{BH}}$  axis, (8) intrinsic logarithmic spread of the data on the y axis as before.

<sup>(a)</sup> Fixed value.

<sup>(b)</sup> In this sample different virial factors for classical/elliptical and pseudo bulges have been used:  $f_{\text{CB}} = 6.3$ ,  $f_{\text{PB}} = 3.2$  (Ho & Kim 2014).

final RM AGN sample is the largest with available bulge classification (Ho & Kim 2015) and hard  $L_X$  and counts a total of 37 sources, 23 of which are elliptical/classical and 14 are pseudo bulges<sup>7</sup>.

We want to calibrate the linear virial relation given in Equation 2, where  $M_{\text{BH}}$  is the RM black hole mass, which is equal to  $f \times M_{\text{vir}}$ ,  $a$  is the zero point and  $b$  is the slope of the average VP. We fitted Equation 2 for the whole sample of RM AGN assuming one of the most updated virial factor  $\langle f \rangle = 4.31$  (Grier et al. 2013), which does not depend on the bulge morphology. The data have a correlation coefficient  $r = 0.838$  which corresponds to a probability as low as  $\sim 9 \times 10^{-11}$  that they are randomly extracted from an uncorrelated parent population. As previously done in Sect. 3, we performed a symmetrical regression fit using FITEXY (Press et al. 2007). We first fixed the slope  $b$  to unity finding the zero point  $a = 8.032 \pm 0.014$ . The resulting observed spread  $\epsilon_{\text{obs}}$  is 0.40 dex, while the intrinsic spread  $\epsilon_{\text{intr}}$  (i.e. once the contribution from the data uncertainties has been subtracted in quadrature) results to be 0.38 dex. We also performed a linear regression, allowing the slope  $b$  to vary. The F-test was carried out to quantitatively verify whether our initial assumption of fixed slope had to be preferred to a relation having free slope. The F-test gave a probability of  $\sim 0.07$  which is not significantly small enough to demonstrate that the improvement using a free slope is not obtained by chance. Therefore, the use of the more physically motivated relation (having slope  $b = 1$ ) that depends only linearly on the VP was preferred. The resulting best-fitting parameters are reported in Table 3, while the virial relation is shown in the top-left panel of Fig. 2 (black solid line).

We then splitted the sample into elliptical/classical (23) and pseudo (14) bulges, adopting the same virial factor  $\langle f \rangle = 4.31$ . The two samples have correlation coefficient  $r > 0.7$  with probabilities lower than  $\sim 10^{-3}$  that the data have been extracted randomly from an uncorrelated parent population (see Table 3). Again we first fixed the slope  $b$  to unity, obtaining the zero points  $a = 8.083 \pm 0.016$  and  $a = 7.911 \pm 0.026$  for classical and pseudo bulges, respectively. We also performed a linear regression allowing a free slope. The F-test was carried out and gave probabilities greater than 0.05 for both the classical and the pseudo

<sup>7</sup> This sample is made of all sources having hard X-ray luminosity measurements among those of Ho & Kim (2014), whose sample of bulge-classified RM AGN includes  $\sim 90\%$  of all the RM black hole masses available in the literature.

bulges samples. Therefore the more physically motivated relations that depend linearly on the VP were preferred, as previously found for the whole sample. Top middle and top right panels of Fig. 2 show the resulting best-fit virial relations for classical (in blue) and pseudo bulges (in red). It should be noted that the average difference between the zero points  $a$  of the two bulge type populations is  $\sim 0.2$  dex.

Obviously, the same fitting results, using these two sub-samples separately, are obtained if the recently determined different  $f$  factors of 6.3 and 3.2 for classical and pseudo bulges (Ho & Kim 2014) are adopted. However, as expected, the difference between the zero points of the two populations becomes larger ( $\sim 0.5$  dex) as the zero points result to be  $a = 8.248 \pm 0.016$  and  $a = 7.782 \pm 0.026$  for the classical and pseudo bulges, respectively.

Finally we performed a calibration of Equation 2 for the whole sample adopting the two virial factors  $f_{\text{CB}} = 6.3$  and  $f_{\text{PB}} = 3.2$ , according to the bulge morphological classification. The data result to have a correlation coefficient  $r = 0.831$  with a probability as low as  $\sim 10^{-10}$  to have been drawn randomly from an uncorrelated parent population. As previously described, we proceeded fixing the slope  $b$  to unity and then fitting a free slope. The F-test gave a probability lower than 0.01, therefore the solution with slope<sup>8</sup>  $b = 1.376 \pm 0.033$  was in this case considered statistically significant (see Table 3). The observed and intrinsic spreads resulted to be  $\sim 0.5$  dex (see Table 3). The bottom panels of Fig. 2 show the virial relations that we obtained for the whole sample (left panel, black dot-dashed line) and separately for classical (middle panel, red dashed line) and pseudo bulges (right panel, blue dotted line), once the two different virial factors  $f$  are adopted according to the bulge morphology.

We note that it is possible to convert our virial calibrations (which were estimated using the mean line widths, once converted into the  $H\alpha$  FWHM, and the mean X-ray luminosity, once converted into the  $L_{2-10\text{keV}}$ ) into other equivalent relations based on either the  $H\beta$ ,  $\text{Pa}\alpha$ ,  $\text{Pa}\beta$  and  $\text{He I}$  FWHM and the  $L_{14-195\text{keV}}$ , by using the correlations shown in Equations 3 and 4. To facilitate the use of our virial BH mass estimators, we list in Table 4 how the virial zero point  $a$  changes according to the couple of variables that one wish to use. Moreover, as shown in the virial relation in the top part of Table 4, it is possible to convert the re-

<sup>8</sup> It should be noted that a slope different than unity implies that the  $L_X - R$  relation ( $R \propto L^\alpha$ ) has a power  $\alpha \neq 0.5$ , contrary to what found by Greene et al. (2010).

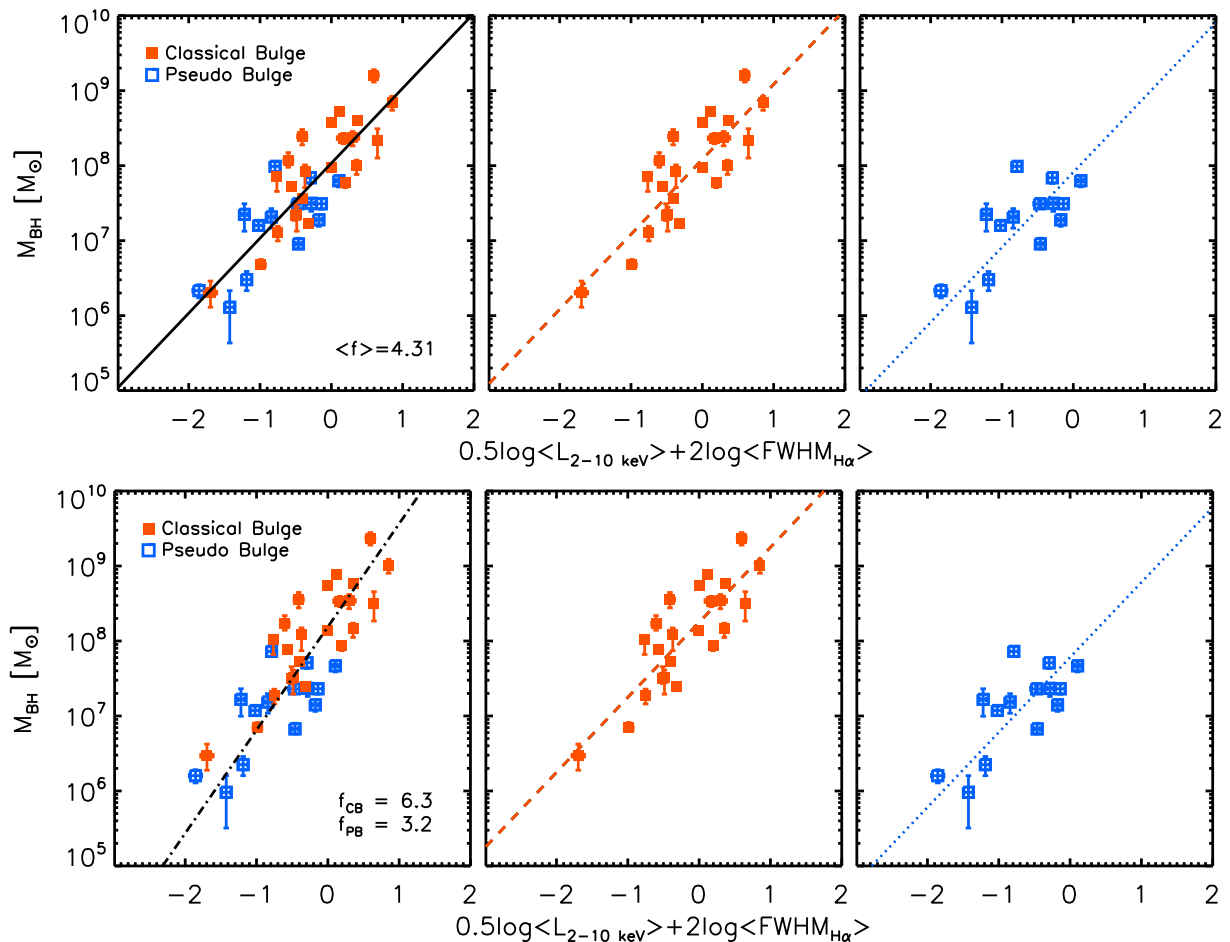


**Fig. 2.** Virial relations between the BH mass  $M_{\text{BH}} = f \times M_{\text{vir}}$  and the average VP given by the mean FWHM (once the  $\text{H}\beta$  has been converted into  $\text{H}\alpha$ ) and the mean  $L_{2-10\text{keV}}$  (using Equation 4 to convert  $L_{14-195\text{keV}}$ ). In the top panels the black hole masses have been calculated assuming  $\langle f \rangle = 4.31$  (Grier et al. 2013), while in the bottom panels two different  $f$ -factors  $f_{\text{CB}} = 6.3$  for classical bulges and  $f_{\text{PB}} = 3.2$  for pseudobulges (Ho & Kim 2014) have been adopted to determine  $M_{\text{BH}}$ . All the VPs are normalized as specified in Equation 2 (see Tables 3-4 for the resulting best-fit parameters). In the left panels the total calibrating sample is shown, while in the middle and right panels the sub-samples of classical (red filled squares) and pseudobulges (blue open squares) are shown separately. The lines show the best-fitting virial relations derived for each sample.

resulting BH masses for different assumed virial  $f$  factors adding the term  $\log(f/f_0)$ , where  $f_0$  is the virial factor that was assumed when each sample was fitted. The values of  $f_0$  are also reported in Table 4 for clarity. Note that, in the last case where a solution was found for the total sample using separate  $f$ -factors for classical and pseudobulges, the  $\log(f/f_0)$  correction cannot be used. However, this last virial relation is useful in those cases where the bulge morphological type is unknown and one wish to use a solution which takes into account the two virial factors for classical and pseudobulges as measured by Ho & Kim (2014). Otherwise, the virial BH mass estimator calculated fitting the whole dataset assuming a single  $\langle f \rangle = 4.31$  can be used (and if necessary converted adopting a different average  $f$  factor).

We compared the virial relation derived by La Franca et al. (2015) using the  $\text{Pa}\beta$  and the  $L_{14-195\text{keV}}$  with our two new virial relations, which depends on the VP given by the  $\text{H}\alpha$  FWHM and the  $L_{14-195\text{keV}}$ , obtained using the total sample, and assuming either 1) an average virial factor  $\langle f \rangle = 4.31$  (as used in La Franca et al. 2015) or 2) the two different  $f$ , separately for classical and pseudobulges. It results that our two new virial relations give BH masses similar to the relation of La Franca et al. (2015) at  $M_{\text{BH}} \sim 10^{7.5} M_{\odot}$ , while they predict 0.3 (0.8) dex

higher BH masses at  $M_{\text{BH}} \sim 10^{8.5} M_{\odot}$  and 0.2 (0.7) dex lower masses at  $M_{\text{BH}} \sim 10^{6.5} M_{\odot}$ , assuming the average  $\langle f \rangle = 4.31$  (the two  $f$ -factors  $f_{\text{CB}} = 6.3$ ,  $f_{\text{PB}} = 3.2$ ). These differences are due to the samples used: our dataset includes 15 AGN with  $M_{\text{BH}} \geq 10^8 M_{\odot}$ , while in the La Franca et al. (2015) sample there are only three, and at  $M_{\text{BH}} \lesssim 10^7 M_{\odot}$  our dataset is a factor two larger.

The same comparison was carried out using the VP given by the  $\text{H}\alpha$  FWHM and the  $L_{2-10\text{keV}}$  with the analogous relation in Bongiorno et al. (2014). All the relations predict similar masses in the  $M_{\text{BH}} \sim 10^{7.5} M_{\odot}$  range, while our new calibrations give 0.1 (0.2) dex smaller (higher) masses at  $M_{\text{BH}} \sim 10^{8.5} M_{\odot}$  and 0.2 (0.1) dex bigger (lower) BH masses at  $M_{\text{BH}} \sim 10^{6.5} M_{\odot}$ , assuming the average  $\langle f \rangle = 4.31$  (the two  $f$ -factors  $f_{\text{CB}} = 6.3$ ,  $f_{\text{PB}} = 3.2$ ).

Finally our analysis shows some similarities with the results of Ho & Kim (2015), who recently calibrated SE optical virial relation based on the  $\text{H}\beta$  FWHM and  $L_{1500}$ , using the total calibrating sample of RM AGN and separated according to the bulge morphology into classical and pseudo bulges. They found that in all cases the  $M_{\text{BH}}$  depends on the optical VP with slope  $b = 1$  and with different zero points  $a$  for classical and pseudobulges. This difference implies that BH hosted in pseudo bulges are pre-

**Table 4.** Final virial BH mass estimators.

$$\log\left(\frac{M_{\text{BH}}}{M_{\odot}}\right) = a + b \left[ 2 \log\left(\frac{\text{FWHM}}{10^4 \text{ km s}^{-1}}\right) + 0.5 \log\left(\frac{L_X}{10^{42} \text{ erg s}^{-1}}\right) \right] + \log\left(\frac{f}{f_0}\right)$$

Variables		All ( $f_0 = 4.31$ )		CB ( $f_0 = 4.31$ )		PB ( $f_0 = 4.31$ )		
$L_X$	FWHM	a	b <sup>(a)</sup>	a	b <sup>(a)</sup>	a	b <sup>(a)</sup>	
(1)	(2)	(3)	(4)	(5)	(6)	(7)	(8)	
a1)	$L_{2-10 \text{ keV}}$	H $\alpha$ (or Pa $\alpha$ , Pa $\beta$ , He I)	$8.03 \pm 0.01$	1	$8.08 \pm 0.02$	1	$7.91 \pm 0.03$	1
a2)	$L_{2-10 \text{ keV}}$	H $\beta$	$7.88 \pm 0.03$	1	$7.93 \pm 0.03$	1	$7.76 \pm 0.04$	1
a3)	$L_{14-195 \text{ keV}}$	H $\alpha$ (or Pa $\alpha$ , Pa $\beta$ , He I)	$7.75 \pm 0.01$	1	$7.79 \pm 0.02$	1	$7.63 \pm 0.03$	1
a4)	$L_{14-195 \text{ keV}}$	H $\beta$	$7.60 \pm 0.03$	1	$7.65 \pm 0.03$	1	$7.48 \pm 0.04$	1

Variables		All <sup>(b)</sup>		CB ( $f_0 = 6.3$ )		PB ( $f_0 = 3.2$ )		
$L_X$	FWHM	a	b	a	b <sup>(a)</sup>	a	b <sup>(a)</sup>	
b1)	$L_{2-10 \text{ keV}}$	H $\alpha$ (or Pa $\alpha$ , Pa $\beta$ , He I)	$8.19 \pm 0.02$	$1.38 \pm 0.03$	$8.25 \pm 0.02$	1	$7.78 \pm 0.02$	1
b2)	$L_{2-10 \text{ keV}}$	H $\beta$	$7.98 \pm 0.04$	$1.38 \pm 0.03$	$8.10 \pm 0.03$	1	$7.63 \pm 0.04$	1
b3)	$L_{14-195 \text{ keV}}$	H $\alpha$ (or Pa $\alpha$ , Pa $\beta$ , He I)	$7.80 \pm 0.02$	$1.38 \pm 0.03$	$7.96 \pm 0.02$	1	$7.50 \pm 0.03$	1
b4)	$L_{14-195 \text{ keV}}$	H $\beta$	$7.59 \pm 0.04$	$1.38 \pm 0.03$	$7.81 \pm 0.03$	1	$7.35 \pm 0.04$	1

**Notes.** Parameters to be used in the virial relation described in the top part of this table. The resulting BH mass values can be converted assuming other virial factor  $f$  using the additional term  $\log(f/f_0)$ . The assumed  $f_0$  in each sample is also reported. All the above virial calibrations have an intrinsic spread of  $\sim 0.5$  dex that should be taken into account when evaluating the accuracy of the BH mass estimates (see Table 3). Columns are: (1) the hard X-ray luminosity, (2) the FWHM, both variables needed to compute the VP, (3) to (8) the zero points  $a$  and the slopes  $b$  of each sample.

<sup>(a)</sup> Fixed value.

<sup>(b)</sup> Note that in this sample different  $f$  factors, according to the bulge morphology, have been adopted. Therefore the average correction  $\log(f/f_0)$  cannot be applied.

dicted to be 0.41 dex less massive than in classical bulges. When we adopt the same  $f$ -factors used by Ho & Kim (2015), we do similarly find that the zero point  $a$  of classical bulges is  $\sim 0.5$  dex greater than for pseudo bulges. However we do not confirm their result obtained using the total sample, as we find that the best-fitting parameter  $b$  of our VP should be different than one. At variance when the same average  $\langle f \rangle = 4.31$  is adopted, both in the total and in the sub-samples of classical and pseudo bulges, we find slope  $b = 1$  relations, while the zero points of classical and pseudo bulges still show an offset of  $\sim 0.2$  dex.

## 5. Discussion and Conclusions

This work was prompted by the results of Ho & Kim (2015) who have calibrated optical different virial relations according to the bulge morphological classification into classical/elliptical and pseudo bulges (Ho & Kim 2014). In order to provide virial relations to be used also for moderately absorbed AGN, following La Franca et al. (2015), we extended the approach of Ho & Kim (2015) using the intrinsic hard X-ray luminosity and NIR emission lines. We thus obtained similar virial relations for the two bulge classes but with an offset between the two zero points of  $\sim 0.2$  dex if the same average  $\langle f \rangle = 4.31$  is used. If instead two different virial factors  $f_{\text{CB}} = 6.3$  and  $f_{\text{PB}} = 3.2$  are assumed, the offset becomes linearly larger by a factor of  $\sim 2$ , confirming the results by Ho & Kim (2015). Neglecting the morphological information leads to a systematic uncertainty of  $\sim 0.2-0.5$  dex, that is the difference we observe when we split the sample according to the host bulge type. This uncertainty will be difficult to eliminate because of the current challenges at play when attempting to accurately measure the properties of the host, especially at high redshift and/or for luminous AGN. As already

stated by Ho & Kim (2015), AGN with  $M_{\text{BH}} \gtrsim 10^8 M_{\odot}$  are most probably hosted by elliptical or classical bulges, as suggested also by the current BH mass measures in inactive galaxies (e.g. Ho & Kim 2014). Similarly,  $M_{\text{BH}} \lesssim 10^6 M_{\odot}$  are very likely hosted in pseudo bulges (e.g. Greene et al. 2008; Jiang et al. 2011). However, the two populations significantly overlap in the range  $10^6 \lesssim M_{\text{BH}}/M_{\odot} \lesssim 10^8$  and therefore without bulge classification the BH mass estimate is accurate only within a factor of  $\sim 0.2-0.5$  dex. Probably accurate bulge/disk decomposition will be available also for currently challenging sources once extremely large telescopes such the EELT become operative for the community. Indeed the high spatial resolution that can be achieved with sophisticated multiple adaptive optics will enable to probe scales of few hundreds of parsecs in the centre of galaxies at  $z \sim 2$  (Gullieuszik et al. 2016).

Obviously, the above results depend on the bulge morphological classification. As discussed in the introduction, this classification should be carried out carefully, and the reliability increases by enlarging the number of selection criteria used (Kormendy & Ho 2013; Kormendy 2016). It should also be noted that according to some authors the main selection criterion should instead be based on the presence or not of a bar (Graham & Li 2009; Graham 2014; Savorgnan & Graham 2015). This simpler selection criterion, which avoids the difficulty arising from the observation that some (at least 10%) galaxies host both a pseudobulge and a classical bulge (Erwin et al. 2003, 2015), is supported by dynamical modelling studies by Debattista et al. (2013) and Hartmann et al. (2014). As a matter of fact it is interesting to remark that an offset of 0.3 dex is also observed in the  $M_{\text{BH}} - \sigma_*$  diagram when the galaxies are divided into barred and unbarred (e.g. Graham 2008; Graham et al. 2011; Graham & Scott 2013). Moreover, Ho & Kim (2014) note that

although the presence of a bar does not correlate perfectly with bulge type, the systematic difference in  $f$  between barred and unbarred galaxies qualitatively resembles the dependence on bulge type that they found.

Recently, Shankar et al. (2016) claimed that all the previously computed  $f$  factors could have been artificially increased by a factor of at least  $\sim 3$  because of a presence of a selection bias in the calibrating samples, in favour of the more massive BHs. This result would imply that all the previous estimate of the virial relations, including those presented in this work, suffer from an almost average artificial offset. If, as discussed by Shankar et al. (2016), the offset is not significantly dependent on  $M_{\text{BH}}$ , then it is sufficient to rescale our results by a correction factor  $\log(f/f_0)$ . The same correction term can also be used to convert our relations assuming virial factors different than those used in this work.

By testing whether the  $H\alpha$  probes a velocity field in the BLR consistent with the  $H\beta$  and the other NIR lines  $\text{Pa}\alpha$ ,  $\text{Pa}\beta$  and  $\text{He I}$ , we widened the applicability of our proposed virial relations. Indeed assuming the virialization of the clouds emitting the  $H\beta$  implies the virialization also of the other lines considered in this work. Moreover, these lines can be valuable tools to estimate the velocity of the gas residing in the BLR also for intermediate (e.g. Seyfert 1.9) and reddened AGN classes, where the  $H\beta$  measurement is impossible by definition. The use of these lines coupled with a hard X-ray luminosity that is less affected by galaxy contamination and obscuration (which can be both correctly evaluated if  $L_X > 10^{42}$  erg  $\text{s}^{-1}$  and  $N_{\text{H}} < 10^{24}$   $\text{cm}^{-2}$ , Ranalli et al. 2003; Mineo et al. 2014), assures that these relations are able to reliably measure the BH mass also in AGN where the nuclear component is less prominent and/or contaminated by the hosting galaxy optical emission. We can conclude that our new derived optical/NIR FWHM and hard X-ray luminosity based virial relations can be of great help in measuring the BH mass in low-luminosity and absorbed AGN and therefore better measuring the complete (AGN1+AGN2) SMBH mass function. In this respect, in the future, a similar technique could also be applied at larger redshift. For example, at redshift  $\sim 2-3$  the  $\text{Pa}\beta$  line could be observed in the 1-5  $\mu\text{m}$  wavelength range with NIRSPEC on the JamesWebb Space Telescope. While, after a straightforward recalibration, the rest-frame 14-195 keV X-ray luminosity could be substituted by the 10-40 keV hard X-ray band (which is as well not so much affected by obscuration for mildly absorbed, Compton Thin, AGN). At redshift  $\sim 2-3$ , in the observed frame, the 10-40 keV hard band roughly corresponds to the 2-10 keV energy range which is typically observed with the Chandra and XMM-Newton telescopes.

*Acknowledgements.* We thank A. Graham whose useful comments improved the quality of the manuscript. Part of this work was supported by PRIN/MIUR 2010NHBSBE and PRIN/INAF 2014\_3.

## References

Baskin, A. & Laor, A. 2005, MNRAS, 356, 1029  
 Baumgartner, W. H., Tueller, J., Markwardt, C. B., et al. 2013, ApJS, 207, 19  
 Bentz, M. C., Denney, K. D., Grier, C. J., et al. 2013, ApJ, 767, 149  
 Bentz, M. C., Peterson, B. M., Pogge, R. W., Vestergaard, M., & Onken, C. A. 2006, ApJ, 644, 133  
 Bentz, M. C., Walsh, J. L., Barth, A. J., et al. 2009, ApJ, 705, 199  
 Bentz, M. C., Walsh, J. L., Barth, A. J., et al. 2010, ApJ, 716, 993  
 Bianchi, S., Guainazzi, B. M., Matt, G., Fonseca Bonilla, N., & Ponti, G. 2009, A&A, 495, 421  
 Blandford, R. D. & McKee, C. F. 1982, ApJ, 255, 419  
 Bongiorno, A., Maiolino, R., Brusa, M., et al. 2014, MNRAS, 443, 2077  
 Burbidge, E. M. & Burbidge, G. R. 1971, ApJ, 163, L21

Cai, H.-B., Shu, X.-W., Zheng, Z.-Y., & Wang, J.-X. 2010, Research in Astronomy and Astrophysics, 10, 427  
 Collin, S., Kawaguchi, T., Peterson, B. M., & Vestergaard, M. 2006, A&A, 456, 75  
 Croton, D. J., Springel, V., White, S. D. M., et al. 2006, MNRAS, 365, 11  
 De Robertis, M. 1985, ApJ, 289, 67  
 Debattista, V. P., Kazantzidis, S., & van den Bosch, F. C. 2013, ApJ, 765, 23  
 Denney, K. D. 2012, ApJ, 759, 44  
 Denney, K. D., Peterson, B. M., Dietrich, M., Vestergaard, M., & Bentz, M. C. 2009, ApJ, 692, 246  
 Di Matteo, T., Springel, V., & Hernquist, L. 2005, Nature, 433, 604  
 Dietrich, M., Peterson, B. M., Grier, C. J., et al. 2012, ApJ, 757, 53  
 Dressler, A. 1989, in IAU Symposium, Vol. 134, Active Galactic Nuclei, ed. D. E. Osterbrock & J. S. Miller, 217  
 Dullo, B. T., Martínez-Lombilla, C., & Knapen, J. H. 2016, MNRAS, 462, 3800  
 Eracleous, M. & Halpern, J. P. 1994, ApJS, 90, 1  
 Eracleous, M. & Halpern, J. P. 2003, ApJ, 599, 886  
 Erwin, P., Beltrán, J. C. V., Graham, A. W., & Beckman, J. E. 2003, ApJ, 597, 929  
 Erwin, P., Saglia, R. P., Fabricius, M., et al. 2015, MNRAS, 446, 4039  
 Fabian, A. C. 1999, MNRAS, 308, L39  
 Fabian, A. C. 2012, ARA&A, 50, 455  
 Ferrarese, L. 2002, in Current High-Energy Emission Around Black Holes, ed. C.-H. Lee & H.-Y. Chang, 3–24  
 Ferrarese, L. & Merritt, D. 2000, ApJ, 539, L9  
 Fisher, D. B. & Drory, N. 2008, AJ, 136, 773  
 Gadotti, D. A. 2009, MNRAS, 393, 1531  
 Gebhardt, K., Kormendy, J., Ho, L. C., et al. 2000, ApJ, 543, L5  
 Gezari, S., Halpern, J. P., & Eracleous, M. 2007, ApJS, 169, 167  
 Graham, A. W. 2008, ApJ, 680, 143  
 Graham, A. W. 2014, in Astronomical Society of the Pacific Conference Series, Vol. 480, Structure and Dynamics of Disk Galaxies, ed. M. S. Seigar & P. T. Barth, 185  
 Graham, A. W. 2016, Galactic Bulges, 418, 263  
 Graham, A. W. & Li, I.-h. 2009, ApJ, 698, 812  
 Graham, A. W., Onken, C. A., Athanassoula, E., & Combes, F. 2011, MNRAS, 412, 2211  
 Graham, A. W. & Scott, N. 2013, ApJ, 764, 151  
 Graham, A. W. & Worley, C. C. 2008, MNRAS, 388, 1708  
 Greene, J. E. & Ho, L. C. 2005, ApJ, 630, 122  
 Greene, J. E., Ho, L. C., & Barth, A. J. 2008, ApJ, 688, 159  
 Greene, J. E., Hood, C. E., Barth, A. J., et al. 2010, ApJ, 723, 409  
 Grier, C. J., Martini, P., Watson, L. C., et al. 2013, ApJ, 773, 90  
 Grier, C. J., Peterson, B. M., Pogge, R. W., et al. 2012, ApJ, 755, 60  
 Grupe, D., Wills, B. J., Leighly, K. M., & Meusinger, H. 2004, AJ, 127, 156  
 Gullieuszik, M., Falomo, R., Greggio, L., Uslenghi, M., & Fantinel, D. 2016, A&A, 593, A24  
 Gültekin, K., Richstone, D. O., Gebhardt, K., et al. 2009, ApJ, 698, 198  
 Haardt, F. & Maraschi, L. 1991, ApJ, 380, L51  
 Haardt, F., Maraschi, L., & Ghisellini, G. 1994, ApJ, 432, L95  
 Haardt, F., Maraschi, L., & Ghisellini, G. 1997, ApJ, 476, 620  
 Hartmann, M., Debattista, V. P., Cole, D. R., et al. 2014, MNRAS, 441, 1243  
 Ho, L. 1999, in Astrophysics and Space Science Library, Vol. 234, Observational Evidence for the Black Holes in the Universe, ed. S. K. Chakrabarti, 157  
 Ho, L. C. & Kim, M. 2014, ApJ, 789, 17  
 Ho, L. C. & Kim, M. 2015, ApJ, 809, 123  
 Hu, J. 2008, MNRAS, 386, 2242  
 Jiang, Y.-F., Greene, J. E., Ho, L. C., Xiao, T., & Barth, A. J. 2011, ApJ, 742, 68  
 Kaspi, S., Smith, P. S., Netzer, H., et al. 2000, ApJ, 533, 631  
 Kim, D., Im, M., Glikman, E., Woo, J.-H., & Urrutia, T. 2015, ApJ, 812, 66  
 Kim, D., Im, M., & Kim, M. 2010, ApJ, 724, 386  
 King, A. 2014, Space Sci. Rev., 183, 427  
 Kollatschny, W., Bischoff, K., Robinson, E. L., Welsh, W. F., & Hill, G. J. 2001, A&A, 379, 125  
 Kollatschny, W., Ulbrich, K., Zetzl, M., Kaspi, S., & Haas, M. 2014, A&A, 566, A106  
 Kormendy, J. 2016, Galactic Bulges, 418, 431  
 Kormendy, J. & Ho, L. C. 2013, ARA&A, 51, 511  
 Kormendy, J. & Richstone, D. 1995, ARA&A, 33, 581  
 La Franca, F., Onori, F., Ricci, F., et al. 2016, Frontiers in Astronomy and Space Sciences, 3, 12  
 La Franca, F., Onori, F., Ricci, F., et al. 2015, MNRAS, 449, 1526  
 Landt, H., Bentz, M. C., Ward, M. J., et al. 2008, ApJS, 174, 282  
 Landt, H., Ward, M. J., Peterson, B. M., et al. 2013, MNRAS, 432, 113  
 Magorrian, J., Tremaine, S., Richstone, D., et al. 1998, AJ, 115, 2285  
 Maiolino, R., Shemmer, O., Imanishi, M., et al. 2007, A&A, 468, 979  
 Marconi, A. & Hunt, L. K. 2003, ApJ, 589, L21  
 Marziani, P., Sulentic, J. W., Dultzin-Hacyan, D., Calvani, M., & Moles, M. 1996, ApJS, 104, 37

- Marziani, P., Sulentic, J. W., Plauchu-Frayn, I., & del Olmo, A. 2013, *A&A*, 555, A89
- McConnell, N. J. & Ma, C.-P. 2013, *ApJ*, 764, 184
- McLure, R. J. & Jarvis, M. J. 2002, *MNRAS*, 337, 109
- Mejía-Restrepo, J. E., Trakhtenbrot, B., Lira, P., Netzer, H., & Capellupo, D. M. 2016, *MNRAS*, 460, 187
- Mineo, S., Gilfanov, M., Lehmer, B. D., Morrison, G. E., & Sunyaev, R. 2014, *MNRAS*, 437, 1698
- Onken, C. A., Ferrarese, L., Merritt, D., et al. 2004, *ApJ*, 615, 645
- Onori, F., La Franca, F., Ricci, F., et al. 2016, *MNRAS*
- Osterbrock, D. E. 1981, *ApJ*, 249, 462
- Ostriker, J. P., Choi, E., Ciotti, L., Novak, G. S., & Proga, D. 2010, *ApJ*, 722, 642
- Park, D., Kelly, B. C., Woo, J.-H., & Treu, T. 2012, *ApJS*, 203, 6
- Peterson, B. M. 1993, *PASP*, 105, 247
- Peterson, B. M., Ferrarese, L., Gilbert, K. M., et al. 2004, *ApJ*, 613, 682
- Piconcelli, E., Jimenez-Bailón, E., Guainazzi, M., et al. 2005, *A&A*, 432, 15
- Press, W. H., Teukolsky, S. A., Vetterling, W. T., & Flannery, B. P. 2007, *Numerical recipes: the art of scientific computing*, 3rd edn. (Cambridge Univ. Press, Cambridge)
- Ranalli, P., Comastri, A., & Setti, G. 2003, *A&A*, 399, 39
- Riffel, R., Rodríguez-Ardila, A., & Pastoriza, M. G. 2006, *A&A*, 457, 61
- Runnoe, J. C., Brotherton, M. S., Shang, Z., & DiPompeo, M. A. 2013, *MNRAS*, 434, 848
- Sabra, B. M., Saliba, C., Abi Akl, M., & Chahine, G. 2015, *ApJ*, 803, 5
- Sani, E., Marconi, A., Hunt, L. K., & Risaliti, G. 2011, *MNRAS*, 413, 1479
- Savorgnan, G. A. D. & Graham, A. W. 2015, *MNRAS*, 446, 2330
- Sersic, J. L. 1968, *Atlas de galaxias australes*
- Shankar, F., Bernardi, M., Sheth, R. K., et al. 2016, *MNRAS*[arXiv:1603.01276]
- Shen, Y. 2013, *Bulletin of the Astronomical Society of India*, 41, 61
- Shen, Y. & Liu, X. 2012, *ApJ*, 753, 125
- Sijacki, D., Springel, V., Di Matteo, T., & Hernquist, L. 2007, *MNRAS*, 380, 877
- Silk, J. & Rees, M. J. 1998, *A&A*, 331, L1
- Tremaine, S., Gebhardt, K., Bender, R., et al. 2002, *ApJ*, 574, 740
- Veilleux, S., Goodrich, R. W., & Hill, G. J. 1997, *ApJ*, 477, 631
- Véron, P., Gonçalves, A. C., & Véron-Cetty, M.-P. 2002, *A&A*, 384 [astro-ph/0201240]
- Vestergaard, M. & Peterson, B. M. 2006, *ApJ*, 641, 689
- Wandel, A., Peterson, B. M., & Malkan, M. A. 1999, *ApJ*, 526, 579
- Woo, J.-H., Treu, T., Barth, A. J., et al. 2010, *ApJ*, 716, 269
- Zu, Y., Kochanek, C. S., & Peterson, B. M. 2011, *ApJ*, 735, 80